# A GB-SAR operating in monostatic and bistatic modalities for retrieving the displacement vector

# A GB-SAR operating in monostatic and bistatic modalities for retrieving the displacement vector

Massimiliano Pieraccini, *Member, IEEE*, Lapo Miccinesi, *Student Member, IEEE*, and Neda Rojhani

***Abstract*—GBSAR (Ground-Based Synthetic Aperture Radar) systems are popular remote sensing instruments for detecting ground changes of slopes, and small displacements of large structures as bridges, dams, construction works. These radars are able to provide maps of displacement along range direction only. In this letter the authors propose to use a transponder for operating a conventional linear GBSAR as a bistatic radar with the aim to acquire two different components of the displacement of the targets in the field of view.**

***Index Terms* — Bistatic radar, GB-SAR, Radar, remote sensing, SAR**

## I. Introduction

SINCE 2003 [1] Ground Based Synthetic Aperture Radar (GBSAR) has been proposed as geotechnical equipment for detecting ground displacements on slopes. Currently many research groups are working in this field and the technique can be considered well-consolidated [2].

These radars are able to provide maps of displacement along the range direction. Nevertheless, Severin et al. [3] demonstrated the great advantage of the vector displacement in slope monitoring, and Dei et al. [4] experimentally showed how the detection of only one component can give paradoxical results in structural monitoring (a bridge deck that apparently is raised when loaded).

In 2014 Crosetto et al. proposed a noninterferometric procedure for detecting the transversal component of the displacement [5]. In 2017 Hu et al. [6] proposed to process two half scans separately for obtaining two images with a baseline. Both methods are limited by the scan length: the larger is the scan the better is the accuracy of the traversal displacement.

In this paper the authors propose to use a transponder for operating a conventional linear GBSAR as a bistatic radar. In this way the same radar equipment is able to acquire two images taken from different points of view: so it is able to acquire two different components of the displacement of the targets. Contrary to works [5],[6] the accuracy in the detection of the transversal displacement does not depend on the scan length (that in a GB-SAR installation can hardly overcome 2-3 m) but on the distance between radar and transponder that can be tens or even hundreds meters.

M. Pieraccini and L. Miccinesi are with Department of Information Engineering (DINFO) of the University of Florence, via Santa Marta, 3 50138 Firenze (Italy) (phone: +390552758581; e-mail: massimiliano.pieraccini@unifi.it).

## II. The bistatic GBSAR working principle

The working principle of the proposed Bistatic GBSAR is shown in Fig. 1. A linear GB-SAR acquires an image of its own field of view. Using a third antenna it acquires a second image of the same scenario exploiting the bouncing of the signal through a transponder. The transponder consists of a couple of antennas and an amplifier.

Bistatic SAR image can be focused through a back projection algorithm [7]. With reference to Fig. 1 the back projection is implemented compensating the phase history of any path radar-target-transponder-radar. On this basis we have modified the algorithm described in [8] (that was originally developed for a monostatic ArcSAR) for operating in the bistatic modality as described above.

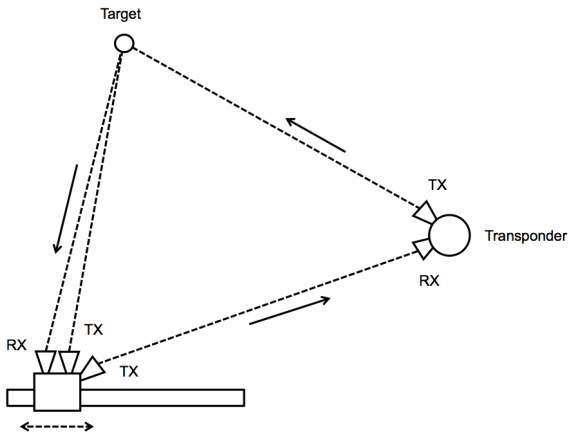


Fig. 1. Working principle of Bistatic GBSAR

The monostatic and bistatic images are focused in the same grid, but generally this does not assure that they are co-registered [9,10], so they could need the application of a specific processing technique for associating the corresponding pixels in the two images. Nevertheless for targets that are smaller than resolution in an environment without heavy clutter, we can assume the two images are co-registered. The experimental set-up has been arranged according to this assumption.

## III. Detecting 2D-displacements

As known, in the monostatic configuration, when a target in

the position $(x_0,y_0)$ is displaced of a vector $\vec{s}$, the electromagnetic path is changed of

$$\Delta l_1 = 2\left(\vec{s}\cdot\vec{u}_1\right) \tag{1}$$

with $\vec{u}_1$ unit vector from the radar to the target position (see Fig. 2).

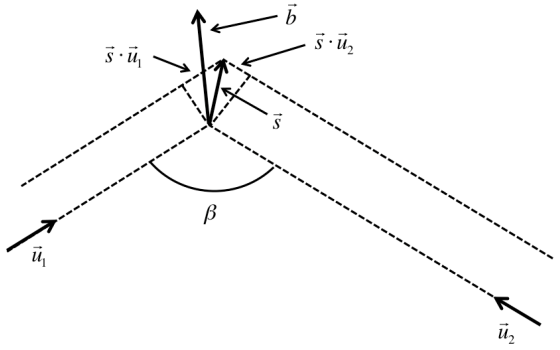


Fig. 2 Detected displacements

Generally speaking a change ($\Delta l$) in the electromagnetic path is detected as phase change ($\Delta\phi$) in the interferogram by the following fundamental relationship

$$\Delta l = \frac{\lambda}{2\pi}\Delta\phi \tag{2}$$

Therefore

$$\Delta s_1 \equiv \vec{s}\cdot\vec{u}_1 = \frac{\lambda}{4\pi}\Delta\phi_1 \tag{3}$$

with $\Delta\phi_1$ differential phase in monostatic configuration. Eq. (3) is the well-known relationship between phase and displacement at the basis of radar inteferometry [1].

In the bistatic configuration when a target in the position $(x_0,y_0)$ is displaced of a vector $\vec{s}$ the electromagnetic path is changed of

$$\Delta l_2 = \vec{s}\cdot\vec{u}_1 + \vec{s}\cdot\vec{u}_2 = \vec{s}\cdot\vec{b}\left|\vec{u}_1+\vec{u}_2\right| = 2\left(\vec{s}\cdot\vec{b}\right)\cos\left(\frac{\beta}{2}\right) \tag{4}$$

where $\vec{u}_1$ and $\vec{u}_2$ are the unit vectors shown in Fig. 1, $\vec{b}$ is the bisector unit vector, and $\beta$ is the bistatic angle.

Therefore

$$\Delta s_2 = \vec{s}\cdot\vec{b} = \frac{\lambda}{4\pi}\frac{1}{\cos\left(\frac{\beta}{2}\right)}\Delta\phi_2 \tag{5}$$

with $\Delta\phi_2$ differential phase in monostatic configuration. The detected displacements $\Delta s_1$ and $\Delta s_2$ are in linear relationship with the two orthogonal components $\Delta x$ and $\Delta y$ of the effective displacement:

$$\begin{pmatrix}\Delta s_1\\ \Delta s_2\end{pmatrix} = M\begin{pmatrix}\Delta x\\ \Delta y\end{pmatrix} \tag{6}$$

with

$$M = \begin{bmatrix}\cos\vartheta_x^{(1)} & \cos\vartheta_y^{(1)}\\ \cos\vartheta_x^{(2)} & \cos\vartheta_y^{(2)}\end{bmatrix} \tag{7}$$

$$\cos\vartheta_x^{(m)} = \frac{\vec{s}_m\cdot\vec{i}}{\left|\vec{s}_m\right|} \quad m=1,2 \tag{8}$$

$$\cos\vartheta_y^{(m)} = \frac{\vec{s}_m\cdot\vec{j}}{\left|\vec{s}_m\right|} \quad m=1,2 \tag{9}$$

where $\vec{i}$ and $\vec{j}$ are the orthogonal basis of the Cartesian plane. Therefore

$$\begin{pmatrix}\Delta x\\ \Delta y\end{pmatrix} = M^{-1}\begin{pmatrix}\Delta s_1\\ \Delta s_2\end{pmatrix} \tag{10}$$

The later equation allows to calculate $\Delta x$ and $\Delta y$ from the measured displacements $\Delta s_1$ and $\Delta s_2$.

In order to assess the measurement error we consider the case depicted in Fig. 3. The target is in front of the radar (along the $y$ direction) and the transponder is on a side. For this geometry the matrix $M$ results

$$M = \begin{bmatrix}0 & 1\\ \sin\left(\frac{\beta}{2}\right) & \cos\left(\frac{\beta}{2}\right)\end{bmatrix} \tag{11}$$

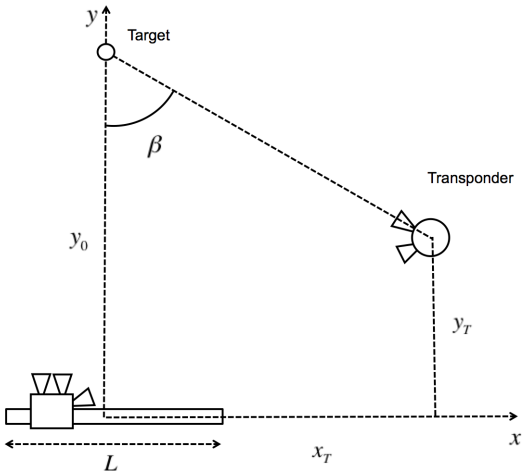


Fig. 3 Measurement geometry

Let $\delta\phi_1$ be the phase uncertainty in monostatic configuration and $\delta\phi_2$ be the phase uncertainty in bistatic configuration, by inverting the matrix M and using eq. (3) and eq. (5), the displacement uncertainty along $y$ ($\delta y$) results

$$\delta y = \frac{\lambda}{4\pi}\delta\phi_1 \tag{12}$$

while the displacement uncertainty along $x$ ($\delta x$) results

$$\delta x = \left|\cot\left(\frac{\beta}{2}\right)\right|\frac{\lambda}{4\pi}\delta\phi_1 + \left|\frac{2}{\sin\beta}\right|\frac{\lambda}{4\pi}\delta\phi_2 \tag{13}$$

Later equation expresses how the uncertainty along $x$-axis depends on bistatic angle $\beta$. It is worth to note that $\delta\phi_1$ and $\delta\phi_2$ can be different, as $\delta\phi_2$ depends on bistatic radar cross section of the target (that is different from monostatic radar cross section) and even on the gain, noise figure, and phase stability of the transponder.

## IV. RADAR AND TRANSPONDER

Fig. 4 shows a sketch of the radar prototype that has been assembled for testing the working principle above described.

A vector network analyzer (VNA) HP8720D operated as transceiver providing a continuous wave stepped frequency

signal (CWSF) in X-band with central frequency $f_c$=10 GHz, bandwidth $B$ = 160 MHz, and number of tones $N_f$= 401. The integration time of each tone was 1 ms. Two RF cables linked the VNA to the front-end that scanned along a mechanical axis of length $L$=1.80 m. The power that fed the antenna was -5dBm. Further details of the system and the antennas have been already reported in [8].

A SPDT (single pole double throw) switched between the TX antenna pointed at the field of view and the TX antenna pointed at the transponder. The radar performed the two acquisitions for each single step along the mechanical rail.

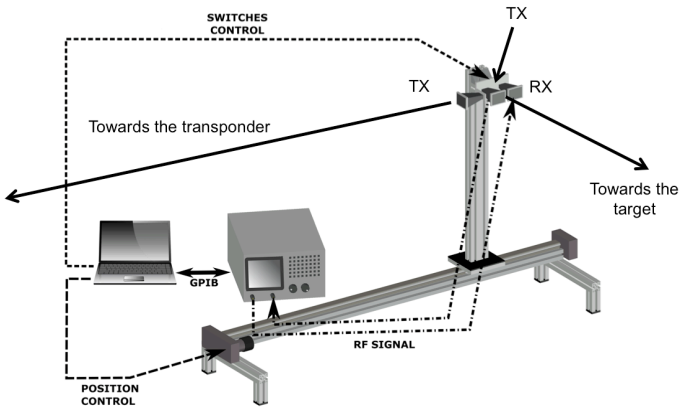


Fig. 4 The radar prototype

The transponder consisted of two horns with 18 dB gain and a wideband amplifier (Nominal gain: 50 dB, Band: 6-18 GHz, Noise Figure: 5 dB) on a tripod.

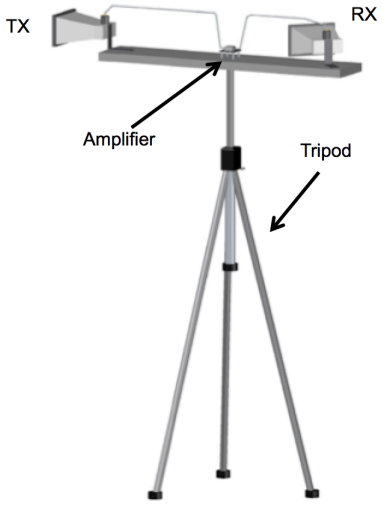


Fig. 5 The transponder

The two antennas could be oriented and they were separated by a length of 1.44 m for minimizing the coupling and the possible oscillation of the transponder.

## V. Experimental Tests

A special target has been assembled aiming to test the capability of the radar to detect two components of the displacement. The target is a metallic pole provided with a small adjustable corner reflector 10 cm × 10 cm and 3 grids disposed orthogonally as shown in Fig. 6. The aim of the grids is to provide a significant bistatic radar cross section. The pole has been mounted on a linear micrometric stage platform with two orthogonal controlled movements on the $x$-$y$ plane with 0.1 mm nominal accuracy and 25 mm of maximum displacement. Some eccosorb has been used to cover the mechanical device. The micrometric stage was fastened to a wood table and a dead load kept the wood table fixed.

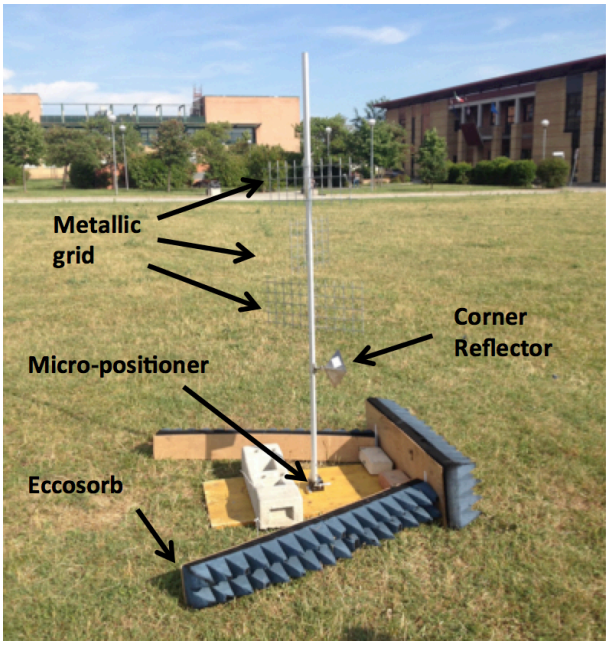


Fig. 6 Picture of the target

The target and the transponder were positioned as shown in Fig. 3. The distance target-radar ($y_0$) was 104.45 m, the coordinates of the transponder were $x_T$= 39.53 m, $y_T$= 45.80 m.

Fig. 7 shows the obtained monostatic image of the scenario where the radar has been installed, compared with an aerial picture. The more evident features are the large building at 300 m in front of the radar, the shack at about 200 m, and the corner of the building at about 130 m on the right. The target appears as a single point.

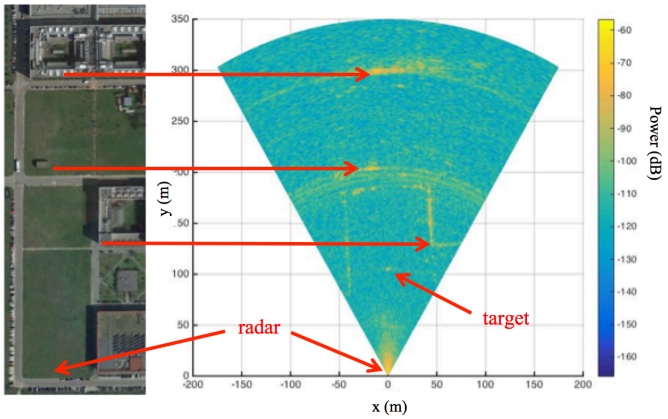


Fig.7 Monostatic radar image

The obtained bistatic radar image of the same scenario is shown in Fig. 8. The target is quite evident as well as a feature (an artifact) that apparently does not correspond to any physical target. This artifact is due to the clutter behind the transponder that can give a monostatic signal even in bistatic configuration. This has been confirmed by focusing in bistatic modality an acquisition carried out when the transponder was switched off (Fig. 9).

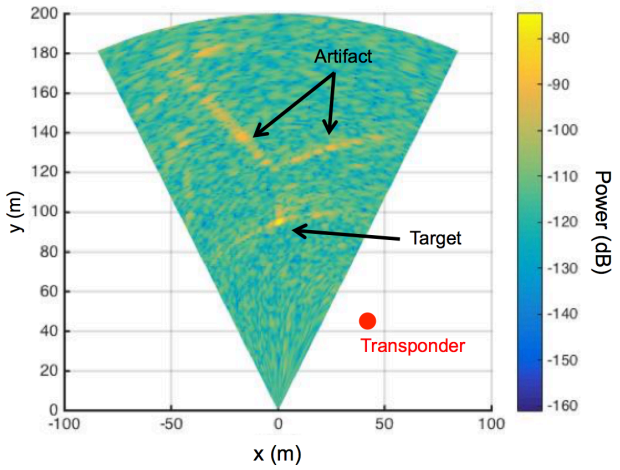


Fig. 8. Bistatic radar image

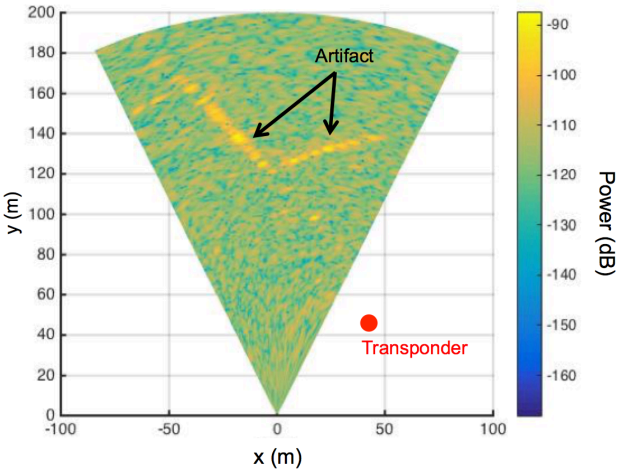


Fig. 9. Bistatic radar image when the transponder was switched off

By focusing the same acquisition in monostatic modality (performed when the transponder was switched off) it is evident that the artifact in bistatic image is due to the building behind the transponder on the right side of the field of view (see Fig. 10).

This suggests a simple procedure for rejecting the artifact: to perform a bistatic acquisition when the transponder is switched on and a second bistatic acquisition when the transponder is switched off. In the subtraction of the two images, the artifact results just a weak residual as shown in Fig. 11.

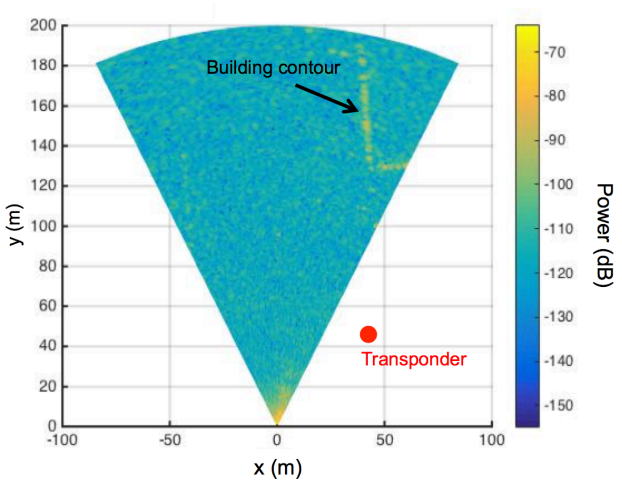


Fig. 10. Radar image obtaining focusing with the monostatic algorithm the bistatic data acquired when the transponder was switched off

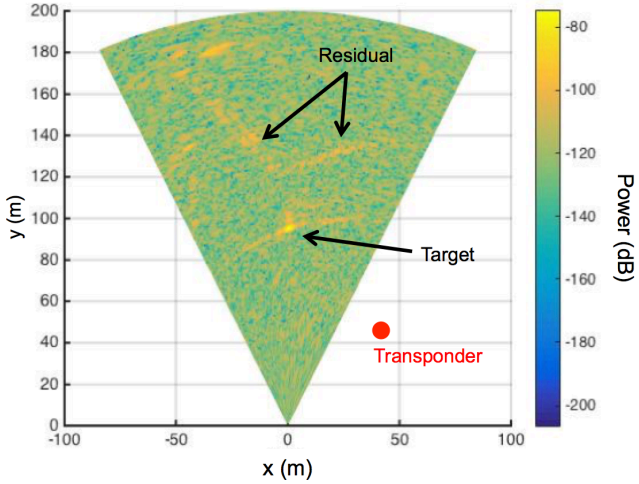


Fig. 11. Bistatic radar image obtaining as subtraction of the images in Fig. 8 and Fig. 9

In order to evaluate the capability of the radar to detect two components of the displacement, the micrometric stage platform carried out displacements along $x$ (toward the positive direction of $x$-axis) at steps of 5.00 mm from 0.00 mm to 25.00 mm.

The $\Delta x$ and $\Delta y$ measured by the radar are shown in Fig. 12. The obtained mean absolute deviation of $\Delta x$ around the nominal value was 1.74 mm, while the deviation of $\Delta y$ was 0.60 mm. By considering each single step as an independent measurement the mean value along x was 5.59 mm (to be compared to the nominal value 5.00 mm) with a standard deviation of 0.84 mm, while the mean value along $y$ was -0.17 mm (to be compared to the nominal value 0.00 mm) with a standard deviation of 0.43 mm.

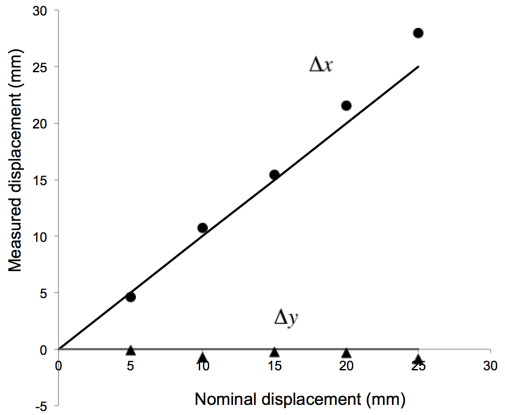


Fig. 12 Displacements along x. The circles are the measured displacements along x and the triangles are the measured displacements along y

In a second measurement session the same micrometric stage platform carried out displacements along $y$ (toward the radar). The target and the transponder were positioned as shown in Fig 3. The target-radar distance ($y_0$) was 75.39 m, the coordinates of the transponder were $x_T$= 35.10 m, $y_T$= 37.53 m. The $\Delta x$ and $\Delta y$ measured by the radar are shown in Fig. 13.

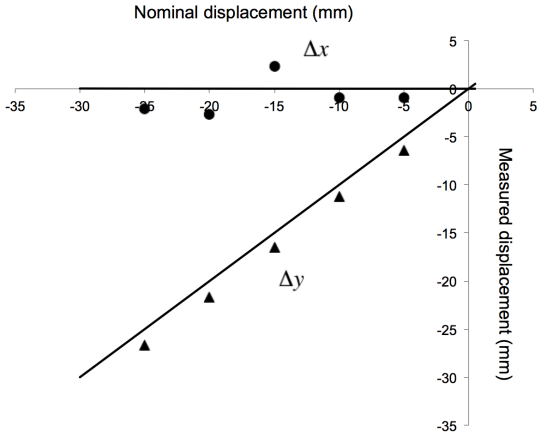


Fig. 13 Displacements along y. The circles are the measured displacements along x and the triangles are the measured displacements along y.

The obtained mean absolute deviation of $\Delta x$ around the nominal value was 2.16 mm, while the deviation of $\Delta y$ was 1.67 mm. By considering each single step as an independent measurement the mean value along x was -0.41 mm (to be compared to the nominal value 0.00 mm) with a standard deviation of 3.02 mm, while the mean value along y was 5.33 mm (to be compared to the nominal value 5.00 mm) with a standard deviation of 0.64 mm.

## VI. Conclusion

In this letter it has been demonstrated that, using a transponder, a monostatic linear GBSAR can operate as a bistatic system. The great advantage of this configuration is its capability to detect two components (or three, using two transponders) of the displacement of the targets in the field of view.

A critical issue of this technique could be the presence of "ghost targets" in the bistatic image, due to the monostatic signal of the clutter behind the transponder. As practical rule, the transponder should not be installed in a position where there are heavy clutter in the background. Nevertheless, an effective countermeasure for rejecting/mitigating the "ghost targets" was to subtract the image acquired when the transponder was off from the image acquired when the transponder was on. Anyway, the scenario can have small changes between the two acquisitions, so a weak residual could remain in the bistatic image.

Another critical issue could be the long term phase stability of the transponder that could affect the displacement measurement. However, both a possible phase change of the transponder amplifier and a small uncontrolled movement of the mechanical support of the transponder can be treated as a change in the atmospheric phase screen and so can be compensated [11],[12].

## References

[1] M. Pieraccini, N. Casagli, G. Luzi, D. Tarchi, D. Mecatti, L. Noferini, C. Atzeni "Landslide monitoring by ground-based radar interferometry: a field test in Valdarno (Italy)." *International Journal of Remote Sensing* Vol. 24, No. 6, pp. 1385-1391, 2003

[2] R. Caduff, F. Schlunegger, A. Kos, A. Wiesmann, A. "A review of terrestrial radar interferometry for measuring surface change in the geosciences." *Earth surface processes and landforms*, Vol. 40, No. 2, pp. 208-228, 2015

[3] J. Severin, E. Eberhardt, L. Leoni, S. Fortin, "Development and application of a pseudo-3D pit slope displacement map derived from ground-based radar." *Engineering Geology*, Vol. 181, pp. 202-211, 2014

[4] D. Dei, D. Mecatti, and M. Pieraccini, "Static Testing of a Bridge Using an Interferometric Radar: The Case Study of ''Ponte degli Alpini,'' Belluno, Italy", *The Scientific World Journal*, Vol. 2013, Article ID 504958, (2013)

[5] M. Crosetto, O. Monserrat, G. Luzi, M. Cuevas-Gonzalez, N. Devanthery, "A noninterferometric procedure for deformation measurement using GB-SAR imagery." *IEEE Geoscience and Remote Sensing Letters*, Vol. 11, No. 1, pp. 34-38, January 2014.

[6] C. Hu, Y. Deng, R. Wang, W. Tian, T. Zeng, "Two-Dimensional Deformation Measurement Based on Multiple Aperture Interferometry in GB-SAR." *IEEE Geoscience and Remote Sensing Letters*, Vol. 14, No. 2, pp. 208-212, February 2017

[7] Y. Ding, D. C. Jr Munson, "A fast back-projection algorithm for bistatic SAR imaging." IEEE International Conference on Image Processing, 22-25 Sept. 2002, DOI: 10.1109/ICIP.2002.1039984

[8] M. Pieraccini, L. Miccinesi, ArcSAR: Theory, Simulations, and Experimental Verification, *IEEE Transactions on Microwave Theory and Techniques*, Vol. 65, No. 1, pp. 293 – 301, January 2017

[9] E. E. Laubie, B. D. Rigling and R. P. Penno, "Bistatic SAR image registration accuracy," 2015 IEEE Radar Conference (RadarCon), Arlington, VA, 2015, pp. 0742-0746.

[10] J. Zhou, Z. Shi and Q. Fu, "Three-Dimensional Scattering Center Extraction Based on Wide Aperture Data at a Single Elevation," *IEEE Transactions on Geoscience and Remote Sensing*, vol. 53, no. 3, pp. 1638-1655, March 2015.

[11] R. Iglesias, X. Fabregas, A. Aguasca, J. J. Mallorqui, C. López-Martínez, J. A. Gili, J. Corominas, "Atmospheric phase screen compensation in ground-based SAR with a multiple-regression model over mountainous regions." *IEEE transactions on geoscience and remote sensing*, Vol. 52, No. 5, pp. 2436-2449, May 2014

[12] L. Iannini, A. Monti Guarnieri, "Atmospheric phase screen in ground-based radar: Statistics and compensation." *IEEE Geoscience and Remote Sensing Letters*, Vol. 8, No. 3, pp. 537-541, May 2011